

Article

A Combined Soda Sintering and Microwave Reductive Roasting Process of Bauxite Residue for Iron Recovery

Chiara Cardenia ^{1,*}, Efthymios Balomenos ^{1,2}, Pritii Wai Yin Tam ^{1,2} and Dimitrios Panias ¹

¹ Zografou Campus, School of Mining and Metallurgical Engineering, National Technical University of Athens, Iroon Polytechniou 9, 15780 Athens, Greece; thymis@metal.ntua.gr (E.B.); pritiit.tam@metal.ntua.gr (P.W.Y.T.); panias@metal.ntua.gr (D.P.)

² Metallurgy Business Unit, Aluminium of Greece Plant, Mytilineos S.A., Agios Nikolaos, 32003 Boeotia, Greece

* Correspondence: chiara.cardenia@yahoo.it; Tel.: +39-32-7201-3400

Abstract: In this study an integrated process is presented as a suitable method to transform Fe³⁺ oxides present in bauxite residue into magnetic oxides and metallic iron through a microwave roasting reduction, avoiding the formation of hercynite (FeAl₂O₄). In the first step, all the alumina phases were transformed into sodium aluminates by adding sodium carbonate as a flux to BR and then leached out through alkali-leaching to recover alumina. Subsequently, the leaching residue was mixed with carbon and roasted by using a microwave furnace at the optimum conditions. The iron oxide present in the sinter was converted into metallic iron (98%). In addition, hercynite was not detected. The produced cinder was subjected to a wet high intensity magnetic separation process to separate iron from the other elements.

Keywords: bauxite residue; microwave roasting process; iron recovery; alumina recovery; soda sintering



Citation: Cardenia, C.; Balomenos, E.; Wai Yin Tam, P.; Panias, D. A Combined Soda Sintering and Microwave Reductive Roasting Process of Bauxite Residue for Iron Recovery. *Minerals* **2021**, *11*, 222. <https://doi.org/10.3390/min11020222>

Academic Editor: Hanumantha Rao Kota

Received: 11 January 2021
Accepted: 19 February 2021
Published: 22 February 2021

Publisher's Note: MDPI stays neutral with regard to jurisdictional claims in published maps and institutional affiliations.



Copyright: © 2021 by the authors. Licensee MDPI, Basel, Switzerland. This article is an open access article distributed under the terms and conditions of the Creative Commons Attribution (CC BY) license (<https://creativecommons.org/licenses/by/4.0/>).

1. Introduction

Microwave roasting process has been examined as an emerging technology of mineral processing. Compared to conventional heat treatment methods, this treatment has different advantages such as significantly faster reaction times and potentially lower energy [1]. These depend on the interaction between material and electromagnetic field generated during the process. The materials can be classified into three different categories based on their dielectric properties. Absorbers are materials that couple microwave energy and easily heat insulators which are transparent to microwave energy and conductors which reflect energy [2–4]. Therefore, microwave energy instantaneously generates heat inside the absorber material, rather than heating the outside surface and slowly conducting it inside [5]. Moreover, microwave heating is a cleaner [6] and more manageable method (quick start-up and stopping) [7] and it offers promising opportunities in terms of energy reducing consumption for intensive firing processes [8]. In the last decades several microwave-based processes have been developed in mineral processing and extractive metallurgy, due to these advantages [1,4,9–11]. In particular, microwave treatment has been employed as an alternative method to recover iron from the bauxite residue (BR) [12–16] which is the solid waste generated during the production of alumina from bauxite ores [6]. Because iron is the major component in BR (14–45 wt.%), several studies were focused on the recovery of iron based on pyrometallurgical processes [17,18]. These works can be classified into two groups: The solid-state reductive roasting followed by magnetic separation [19–23] and the reductive smelting process by using different furnaces (blast furnace, electric arc furnace (EAF), and other types) [24–30]. However, the drawbacks related to these approaches have driven the research to find an innovative method to recover iron from BR. Nowadays, a microwave process is an innovative technology utilized in mineral processing.

In a previous study [31] a microwave reductive roasting process was optimized to transform hematite (Fe_2O_3) and goethite ($\text{Fe}_2\text{O}_3 \cdot \text{H}_2\text{O}$) present in the bauxite residue BR, into magnetite (Fe_3O_4), wüstite (FeO), and metallic iron (Fe^0). During the microwave roasting process, the formation of hercynite (FeAl_2O_4) in the sinter was observed. As Lu et al. [32] explained in their work, hercynite is an unavoidable product. During the roasting process, a carbon source was utilized to reduce hematite can to magnetite [19,20,31], but the presence of alumina in the sample favored the formation of hercynite. Due to its paramagnetic properties [33], iron aluminum oxide can be considered a drawback for the magnetic separation process, since its presence in the magnetic fraction could reduce its purity.

Soda sintering process is covered extensively in many previous studies by Kaußen et al. [34,35], Zheng et al. [36], Alp et al. [37], Meher et al. [38,39] many more which is covered in Tam et al. [40] literature review section as there is potential in removing aluminum and sodium by transformation into sodium aluminate phase, removing two major components and impurities that affect other element recoveries downstream. In literatures that were focused on the carbothermic pig iron recovery from redmud, it was noted that high alkali content, despite reducing melting point, contributes further to furnace lining destruction due to higher reactivity described by researchers such as Valeev et al. [26], Grafe et al. [41], Kaußen et al. [42,43], Borra et al. [28], Anisonyan et al. [44], and Ning et al. [45].

Therefore, the step of removing of aluminum and sodium have been proposed and completed in the previous studies by Tam et al. [40,46,47] using the soda sintering process of bauxite residue with sodium carbonate, which is then leached in mild alkaline solution due to the formation of leachable aluminum and sodium phases in the sinters. This produces leaching residue void of aluminum and sodium which have been optimized for the use of this study.

The aim of this paper is to propose an integrated process composed of three main stages. Firstly, the soda roasting process of BR is taking place to transform all the alumina phases into soluble sodium aluminates which are leached out in alkaline solutions to recover alumina [22,47–53]. In the second stage, the leaching residue is mixed with a metallurgical coke and treated in a microwave furnace at optimum conditions [31]. After this treatment, Fe^{3+} oxides are transformed into magnetic iron oxides and Fe^0 . In the final stage, the produced sinter is subjected to magnetic separation process by using a wet high intensity magnetic separator to recover iron leaving behind the other elements.

2. Materials and Methods

2.1. Bauxite Residue

Bauxite residue used as the main raw material, was provided by Mytilineos, Metallurgy Business Unit (formerly known as AoG). The sample was firstly homogenized by using laboratory sampling procedures (riffing method) and then a representative sample was dried in a static furnace at 105 °C for 24 h. Subsequently, the material was milled using a vibratory disc mill and the sample was fully characterized.

Chemical analyses of major and minor elements were executed via XRF glass disk fusion method with lithium tetraborate in AoG. 1 g of BR sample is fused as melt in platinum crucible with 1 g LiNO_3 oxidizer, and mixture of flux [40].

Mineralogical phases were detected by X-ray diffraction analysis (XRD) using a Bruker D8 Focus powder diffractometer with nickel filtered $\text{CuK}\alpha$ radiation ($\lambda = 1.5405 \text{ \AA}$) coupled with XDB Powder Diffraction Phase Analytical System version 3.107 which evaluated the quantification of mineral phases via profile fitting specifically for bauxite ore and bauxite residue [40,54].

The microstructure of the samples as well as their elemental analysis and distribution, were examined through a scanning electron microscope JEOL 6380LV (SEM) (JEOL, Tokyo, Japan) combined with an Oxford INCA energy dispersive spectrometer (EDS). The particle

size analysis was investigated by using a Malvern Mastersizer TM Laser particle size analyzer (Malvern Instruments, Malvern, UK).

2.2. Soda Sintering/Leaching Process

Dried homogenized bauxite residue was sintered in muffle furnace with 50% excess of sodium carbonate (Na_2CO_3 , Sigma Aldrich, > 99.5% Purity) from stoichiometric amount required for sodium aluminate conversion, which amounted to 25 g Na_2CO_3 for 100 g of bauxite residue. Sintering was performed in alumina crucibles at 900 °C for 2 h duration and left to cool overnight [40]. The sinter leaching experiments were conducted in a 1 L borosilicate glass reactor (Schott AG, Mainz, Germany), equipped with heater (Fibroman-C, 410 W, Saveen & Werner, Limhamn, Sweden), and temperature controller (Glas-Col, thermocouple type-K) as it shown in Figure 1. The sinter was stirred in 0.1 M NaOH solution at 80 °C for 4 h with 1.5% w/v pulp density at 240 rpm stirring rate. Aluminum and sodium were recovered into leachates from the leaching step, leaving solid residue that was further dried in a static oven (105 °C), which produced the modified BR (MBR) used in the next processing steps.

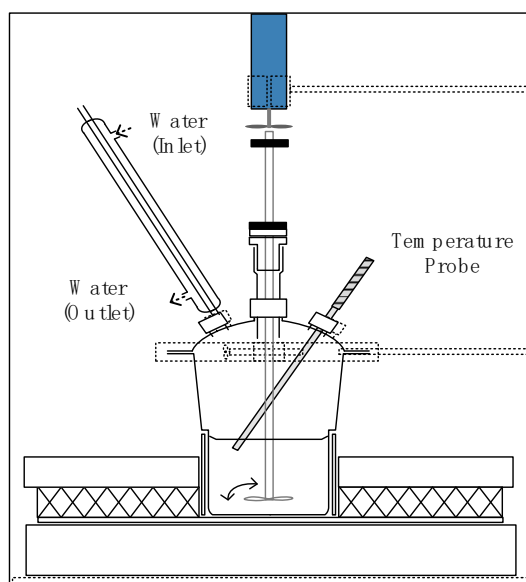


Figure 1. A schematic diagram of leaching reactor.

2.3. Microwave Reductive Roasting Process

Figure 2 shown schematically the 2-kW microwave furnace (Fricke und Mallah Microwave Technology GmbH, Peine, Germany) used for the roasting process experiments.

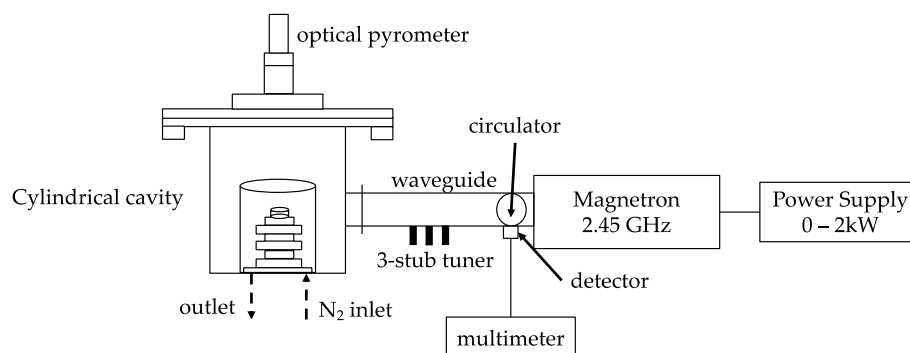


Figure 2. Schematic diagram of the microwave furnace.

A 2.45 GHz air-cooled magnetron converts electrical energy into high frequency microwaves and the power capacity can be set, from 0 kW (0%) to 2 kW (100%). The microwave energy propagated through the rectangular waveguide to the single mode cavity, where the sample is located on the top of a tower (7 cm height and 3 cm length) and placed at the center of the cylindrical cavity.

The 3-stubs tuner present in the waveguide allowed to modify microwave energy to permit the highest coupling between sample and microwave energy for the entire experimental period.

Due to the characteristics of the sample produced, MBR was mixed with a carbon source (metallurgical coke), transforming the powder in tablets (2 cm × 2 cm × 3 mm dimensions and 10 g approximate weights) by using a manual hydraulic press.

To record the temperature during the whole reaction period an optical pyrometer, IMPAC Pyrometer IGA 6/23 Advanced with a RS 485 converter LumaSense Technology (Frankfurt, Germany), was located on the top of the chamber. Moreover, nitrogen flow of 1 L/min was maintained throughout the experiments to ensure inert atmosphere during the reduction of Fe³⁺ oxide into Fe²⁺ oxide and metallic iron.

Zhiyong Xu method was employed to characterize the content of metallic iron (with a tolerable error ranged below 1 wt.%) while AAS and XRF were utilized for the chemical analysis [54].

For the magnetic separation experimental tests, a Carpco Model MWL-3465 laboratory, high-intensity, wet magnetic separator (WHIMS) manufactured by Carpco™ Research and Engineering, Inc. of Jacksonville, FL was utilized (Figure 3) [15].

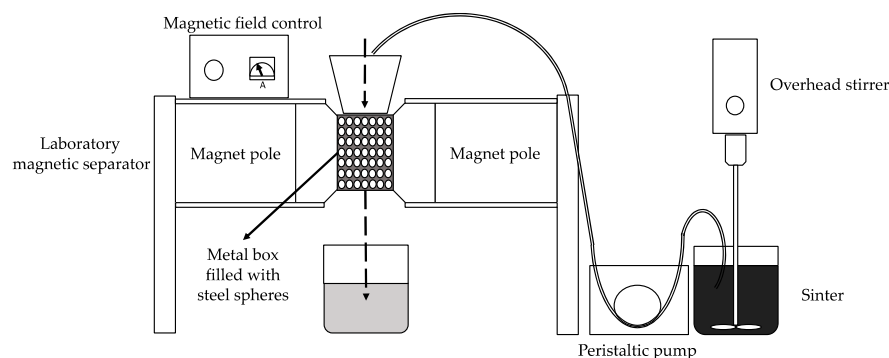


Figure 3. Carpco Model MWL-3465 laboratory, high-intensity, wet magnetic separator schematic diagram.

An intensive magnetic field was generated through two magnet poles by applying a controlled electric field. Due to the high magnetic properties of the cinder, two current settings (0.005 A and 0.01 A) were set for the whole test's duration.

A metal box was placed between the poles and filled with steel spheres during separations. The spheres served as induced magnetic poles and created a point with an intense magnetic field.

At the bottom of the metal box a stainless-steel slide was placed to carry the non-magnetic flux in a beaker.

Magnetic separation experiments were carried out by dispersing the roasting cinder in the water (50 g of cinder in 800 mL of distilled water). The pulp was constantly stirred with an ES Overhead stirrer (VELP SCIENTIFICA, Monza, Italy) at 400 revolutions per minute (rpm) and passed throughout the metal box by using a peristaltic pump with a flow rate of 10 mL/min. The pulp was separated into the magnetic material, which was held to the steel spheres, and the non-magnetic material that passed through the separation zone.

The main purpose of the magnetic separation was to remove the iron-based components in the roasting cinder and concentrate them in the magnetic product. To achieve the target, the feed was treated through the WHIMS two times.

In the first step, a magnetic fraction (MAG I) was collected by employing a 0.005 A current intensity, while a non-magnetic fraction was run again through WHIMS. In the second pass the current intensity was increased to 0.01 A and a second magnetic fraction was gathered (MAG II).

Magnetic I, Magnetic II, and Non-magnetic fractions (residue from second pass, NM) were then dried in a static furnace at 105 °C for 24 h and characterized by using the analytical techniques above mentioned.

3. Results

3.1. Characterization of Bauxite Residue and Metallurgical Coke

Table 1 presented the chemical analysis results of the BR. The main content is attributed to iron oxide (Fe_2O_3) with 43.51 wt.% followed by aluminum oxide (19.25 wt.%), calcium oxide (9.58 wt.%), silicon oxide (6.50 wt.%), titanium oxide (5.49 wt.%) and sodium oxide (2.80 wt.%). the content of rare earths elements (REEs) content, as oxides, is attest to 0.19 wt.%, while the LOI value is 9.41 wt.% due to dehydration and decarbonation of mineral phases existing in the residue.

Table 1. Chemical analysis of bauxite residue.

Sample	Fe_2O_3	Al_2O_3	SiO_2	TiO_2	Na_2O	CaO	REEs	Others	LOI
Bauxite residue (wt.%)	43.51	19.25	6.50	5.49	2.80	9.58	0.19	3.27	9.41

The quantification analysis carried out with the XDB software confirmed that hematite is the main mineral in BR with 30 wt.%. The other iron mineralogical phases were calcium aluminum iron silicate hydroxide, goethite, and chamosite with 17 wt.%, 9 wt.%, and 4 wt.% respectively. The mineralogical phases of BR are presented in Table 2.

Table 2. Bauxite residue mineralogical phases.

Minerals	Formula	wt.%
Hematite	$\alpha\text{-Fe}_2\text{O}_3$	30
Goethite	$\text{Fe}_2\text{O}_3\cdot\text{H}_2\text{O}$	9
Boehmite	$\gamma\text{-AlOOH}$	3
Diaspore	$\alpha\text{-AlOOH}$	9
Gibbsite	$\text{Al}_2\text{O}_3\cdot 3\text{H}_2\text{O}$	2
Calcite	CaCO_3	4
Anatase	TiO_2	0.5
Rutile	TiO_2	0.5
Perovskite	CaTiO_3	4.5
Cancrinite	$\text{Na}_6\text{Ca}_2(\text{AlSiO}_4)_6(\text{CO}_3)_2$	15
Calcium aluminum iron silicate hydroxide	$\text{Ca}_3\text{AlFe}(\text{SiO}_4)(\text{OH})_8$	17
Chamosite	$(\text{Fe}^{2+},\text{Mg})_5\text{Al}(\text{AlSi}_3\text{O}_{10})(\text{OH})_8$	4
Sum		98.5

Laser particle size analyzer showed the particle size distribution of the dried sample where the mean particle size (D_{50}) of the ground material was 1.87 μm , while 90% of the particles (D_{90}) were below 42.87 μm [31].

The chemical analysis results of metallurgical coke presented in Table 3. The main component of the sample is carbon with 80.31 wt.% and for its high fixed carbon (Fixed C) content, metallurgical coke was selected as the reductant in the microwave roasting process experiments.

Table 3. Metallurgical coke chemical analysis.

Sample	Fe ₂ O ₃	SiO ₂	CaO	MgO	Al ₂ O ₃	TiO ₂	Na ₂ O	Fixed C	S	P	H ₂ O Moist	LOI	Others
Metallurgical coke (wt.%)	0.83	3.42	1.26	0.14	1.91	0.10	0.16	80.31	0.77	0.03	3.31	7.38	0.39

3.2. Soda Sintering Process and Alkaline Leaching

Figure 4 shows the mineralogical alteration of the bauxite residue after soda sintering process and mild alkaline leaching process. During the sintering step, aluminum bearing species such as boehmite, diaspore, gibbsite, and complex phases such as cancrinite are transformed into sodium aluminate (NaAlO₂) [39]. This phase is leached out after the mild alkaline leaching step, and about 70% of all Al is extracted from bauxite residue. Na is also co-extracted at about 85.5%, leaving the leaching residue enriched with Fe as well as Ti for downstream processing [39]. Titanium is concentrated in the form of perovskite. Hematite is found in the leached residue, while new mineralogical phases are detected in the modified BR: Sodium aluminum silicate (NaAlSiO₄), sodium ferrotitanate (NaFeTiO₄) and harmunite (CaFe₂O₄). Table 4 shows the compositions in element wt.% basis of original bauxite residue (BR), Na₂CO₃ sintered BR and leaching residue (modified BR).

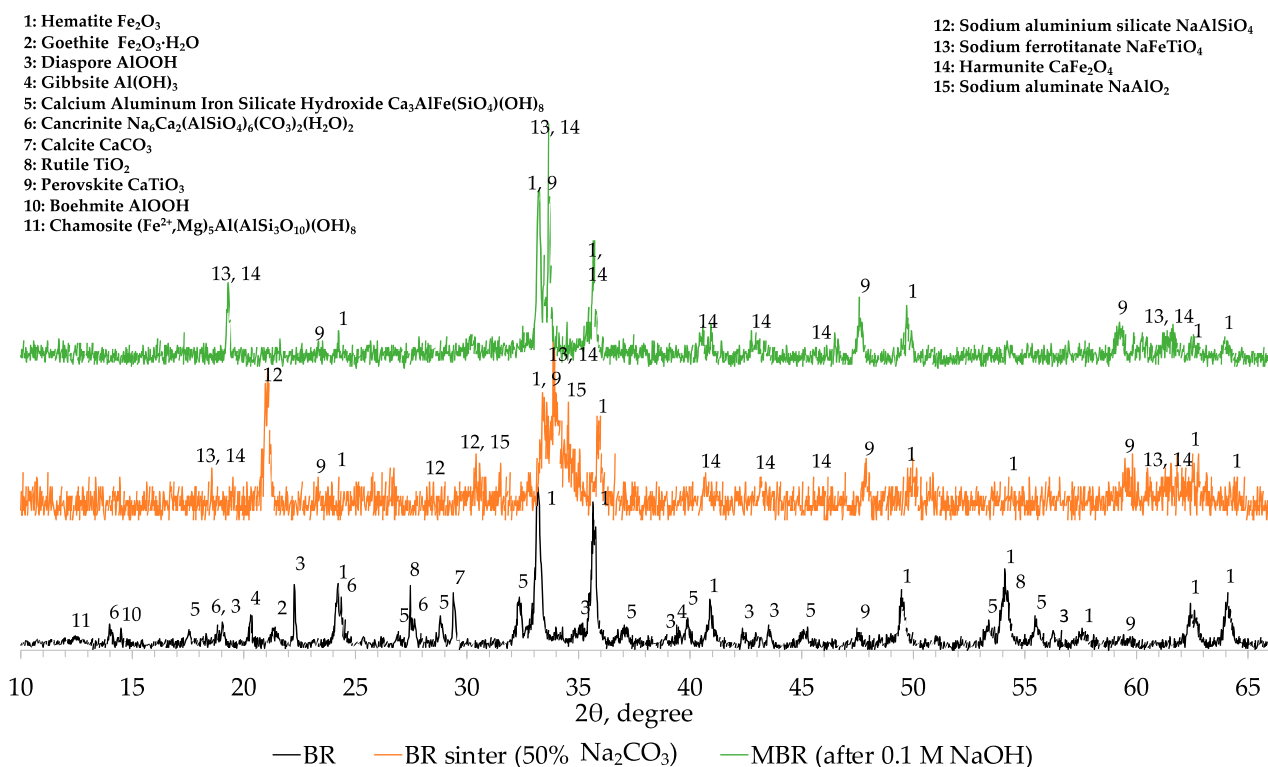


Figure 4. Comparison of the XRD profile of bauxite residue, sinter after bauxite residue sintering sintered with sodium carbonate and modified BR after mild alkaline leaching (0.1 M NaOH) of sinter.

Table 4. Chemical analysis of bauxite residue, sinter and leaching residue (MBR).

Sample	Fe	Al	Si	Ti	Na	Ca	LOI
Bauxite residue (wt.%)	30.43	10.19	3.04	3.29	2.08	6.85	9.40
Sinter (wt.%)	27.72	9.35	2.83	2.82	14.16	6.32	2.73
Leaching residue (modified BR) (wt.%)	37.47	3.83	3.25	3.64	2.86	8.53	9.66

3.3. Microwave Roasting Process of Modified Bauxite Residue

The dried modified BR (MBR) was blended with metallurgical coke at a mass ratio C/MBR 0.225 and it was transformed in tablets using a manual hydraulic press. The sample was treated through microwave roasting process at optimum conditions (0.6 kW, 1 L/min N₂ flow constant and 300 s) and then was characterized via ED-XRF, XRD, and SEM analyses [31].

During the microwave heating of the sample, an immediate absorption was detected, and the temperature almost instantaneously rose within some seconds to 1250 °C (Figure 5).

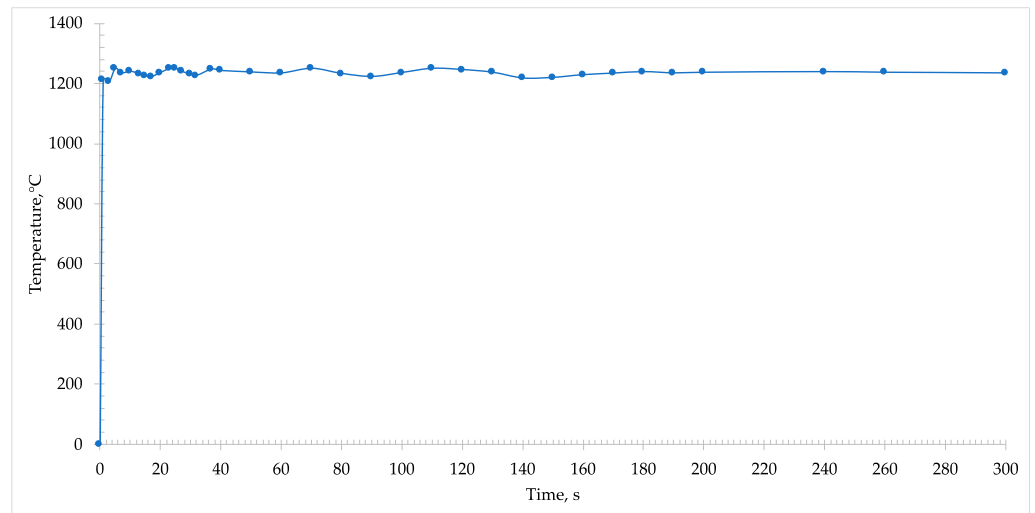


Figure 5. Heating rates of 1st MW roasting process at 0.6 kW, 1 L/min N₂ flow constant and 300 s.

The formation of melt phases was observed through the window of the pyrometer and started from the center and propagated to the rim of the disk. In addition, at this temperature it was possible to note the reduction of iron oxide into metallic iron. In Figure 6 the cinder after the microwave roasting reduction is presented, and the presence of metallic iron nuggets is evident.



Figure 6. Cinder after 300 seconds, irradiation time at 0.6 kW, C/MBR 0.225 and 1 L/min nitrogen flow.

SEM analysis of the cinder confirmed the presence of the spherical metallic particles which are entrapped in the matrix of the solid samples (Figure 7a). The nuggets are covered by a layer of powder (Figure 7b), which has the same composition of the matrix (Ca, Al, Si, Na, Ti and Fe) as it is shown in Figure 7c.

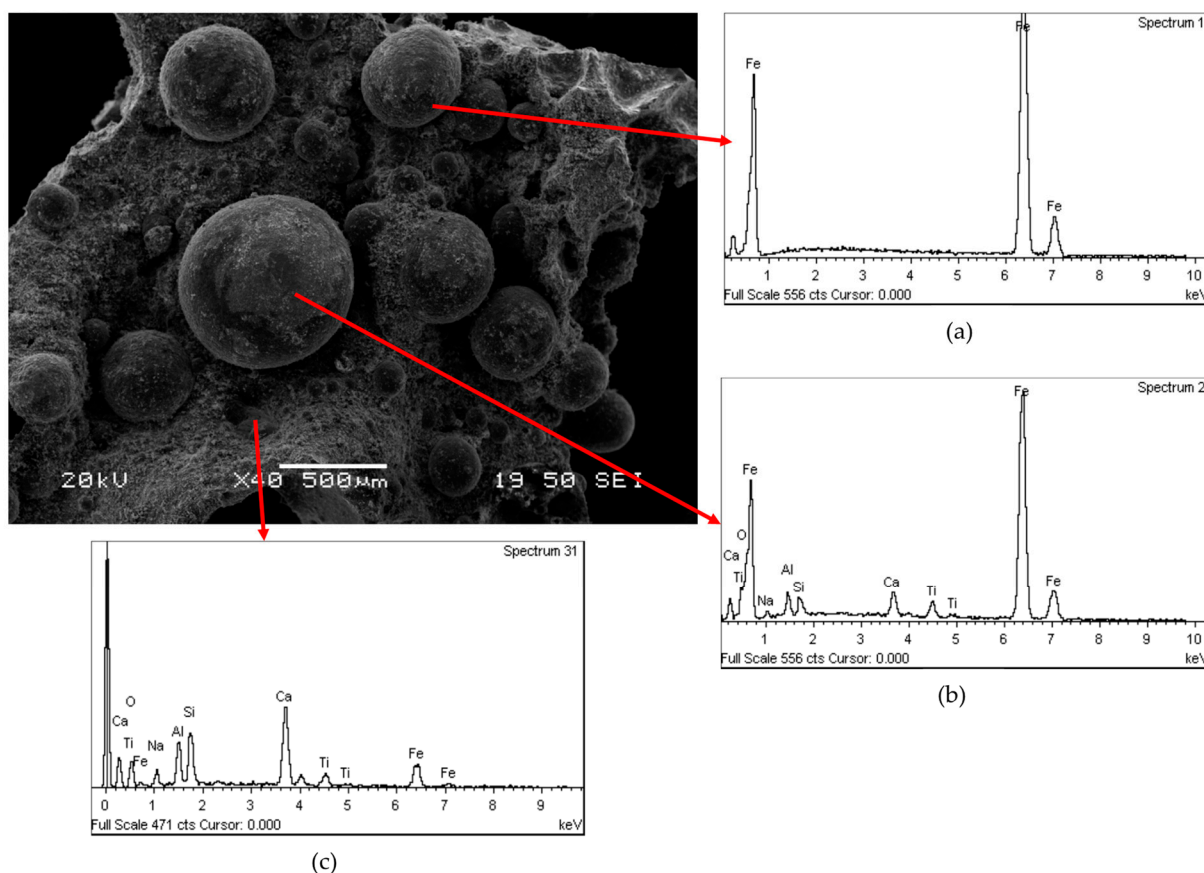


Figure 7. SEM-EDS analysis of cinder after the first microwave roasting reduction: (a) spherical metallic particles, (b) layer of powder on the metallic particles (c) matrix.

To release the metallic iron spheres, the sample was milled using a planetary ball mill (Planetary Ball Mill PM 100–RESTCH, Haan, Germany) with a grinding time of 5 min and a speed a 400 rpm (revolutions per minute). The sample was treated four times with the planetary ball mill to transform the cinder into fine powder. The metallic iron was then separated from the matrix by employing a manual sieve. The sample was, therefore, physically separated into two fractions: The first one with a particle size higher than 0.2 mm mostly composed by Fe nuggets (around 7 wt.% of the total solid sample) and the other one with a particle size lower than 0.2 mm (around 93 wt.% of the total solid sample).

Samples were analyzed via fusion method; chemical composition of the fraction with the particle size higher than 0.2 mm and the other fraction is shown in Table 5.

Table 5. Chemical analysis of the metallic iron spheres fraction with a particle size >0.2 mm and 1st cinder fraction with a particle size lower than 0.2 mm.

Sample	Fe	Al	Si	Ti	Na	Ca	C
>0.2 mm wt. %	95.84	0.01	0.54	0.45	0.01	1.38	
1st cinder fraction (<0.2 mm) wt. %	35.26	4.33	3.63	4.08	3.23	9.54	8.35

Chemical analysis confirmed that the main component of the fraction with particle size higher than 0.2 mm is metallic iron, being more than 95 wt.% of the total weight of

this fraction. In addition, the other fraction (<0.2 mm) still contains a considerable amount of iron.

Analyzing the Fe mass balance, from 35.53 g of Fe present in MBR, 29.59 g of Fe are present in the 1st MW cinder while 5.94 g in the > 0.2 mm fraction.

Comparing the XRD profiles of BR, modified BR and the 1st cinder fraction with a particle size lower than 0.2 mm (Appendix A, Figure A1), the results obtained with chemical and SEM analyses were confirmed. In fact, magnetite (Fe_3O_4) and metallic iron (Fe^0) are the main iron mineralogical phases after the microwave roasting reduction at the optimum conditions (C/MBR 0.225, 0.6 kW, 1 L/min N_2 flow constant and 300 s). Hercynite (FeAl_2O_4) is a mineralogical phase that is not formed during microwave reductive roasting of aluminum depleted MBR materials (Appendix A, Figure A1).

Decreasing the concentration of aluminum in the MBR sample, hematite and other iron-bearing phases are directly reduced into magnetite and then due to the high temperature into metallic iron. At the same time, under these conditions, small part of sodium aluminum silicate (NaAlSiO_4) existing initially in MBR is transformed to anorthite ($\text{CaAl}_2\text{SiO}_3$) as well as gehlenite ($\text{Ca}_2\text{Al}(\text{AlSiO}_7)$) but the major amount of aluminum in cinder remains in the form of sodium aluminum silicate (NaAlSiO_4) (Appendix A, Figure A1). In the 2-theta range of 22 to 28°, the mineralogical characterization revealed the formation of a glassy region indicated by the hump and consisting of calcium silicate (CaSiO_3) and anorthite. Titanium phases are converted into perovskite already from the soda roasting process and remain unchanged during the MW reductive roasting process having been beneficiated in the resulted cinder.

Since the cinder fraction with a particle size lower than 0.2 mm contained good microwave receptors (mineralogical phases such as Fe_3O_4 and C), the sample was subjected for a second time to a microwave roasting process at the same optimum condition (0.6 kW, 1 L/min N_2 flow constant and 300 s), following the already described procedure.

During irradiation with microwaves, an immediate absorption from the sample was detected and the temperature rose within some seconds to 1230 °C (Figure 8).

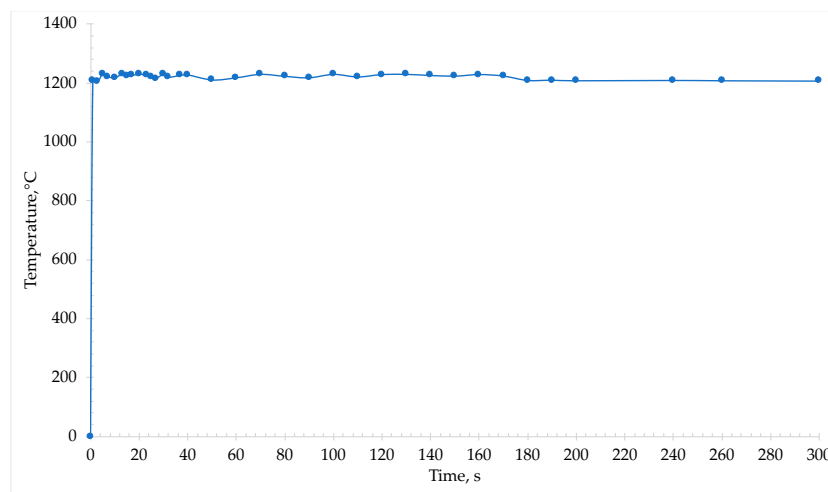


Figure 8. Heating rates of 2nd MW roasting process at 0.6 kW, 1 L/min N_2 flow constant and 300 s.

At this temperature it was possible to note the reduction of iron oxide into metallic iron and the formation of metal phase. Macroscopically, the 2nd cinder appeared similar to the one from the first microwave treatment, but the iron nuggets were smaller in size.

In Figure 9a back-electron scattering (BEC) picture of the 2nd cinder is shown together with EDS chemical analysis on specific components. The light gray spherical particles are metallic iron particles which are entrapped in the matrix that is mainly composed from all the other elements (Ca, Al, Si, Na, Ti, and Fe) (Figure 9b). On the top of the metallic spheres are present also some dark gray particles with the same composition of the matrix (Figure 9c).

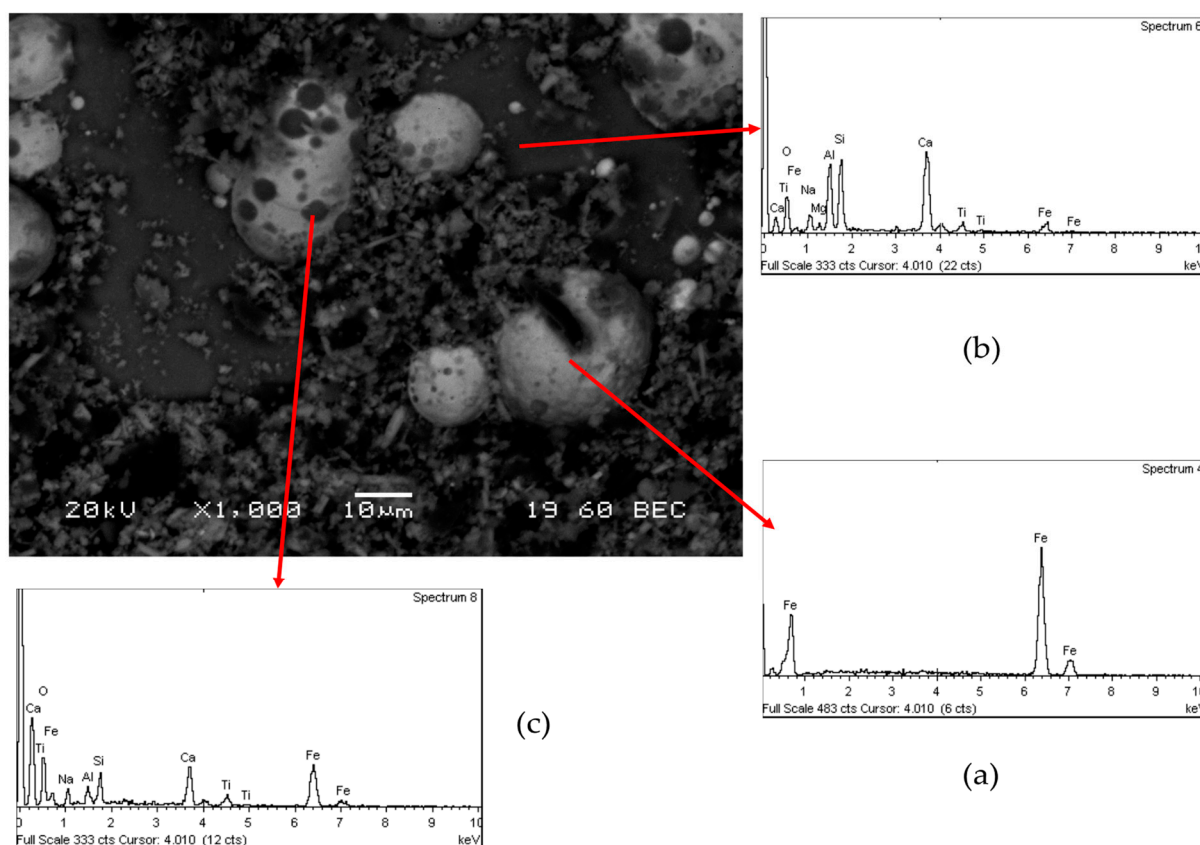


Figure 9. Back electron scattering mode SEM-EDS analysis of the 2nd cinder after the second microwave roasting reduction: (a) metallic spheres (b) matrix (c) dark gray particle on the metallic spheres surface.

The 2nd cinder was ground to release the metallic iron spheres. In this case, for the physical separation, a sieve with openings size of 0.1 mm was used. The chemical analysis of the two fractions formed are presented in Table 6.

Table 6. Chemical analysis of the metallic iron spheres fraction with a particle size > 0.1 mm and of the fraction with a particle size < 0.1 mm.

Sample	Fe	Al	Si	Ti	Na	Ca	C
>0.1 mm wt.%	93.30	0.01	0.42	0.51	0.08	1.70	
2nd cinder fraction (<0.1 mm) wt.%	37.91	4.77	4.00	4.49	3.56	10.49	1.00

Table 6 shows that the main component of the fraction with particle size ≥ 0.1 mm, which is 1 wt.% of the total cinder weight, is metallic iron.

The other fraction, which is the 99 wt.% of the total cinder weight, still contains a considerable amount of iron. Analyzing the Fe mass balance, from 29.59 g of Fe present in the 1st MW cinder, 28.87 g of Fe are present in the 2nd MW cinder while 0.71 g in the >0.1 mm fraction.

The XRD analysis (Appendix A, Figure A2) revealed a mineralogical conformation similar to the one presented in Figure 9, where magnetite (Fe_3O_4) and metallic iron (Fe^0) were the main iron mineralogical phases after the second microwave roasting reduction. The other elements are present in form of anorthite ($\text{CaAl}_2\text{SiO}_3$) gehlenite ($\text{Ca}_2\text{Al}(\text{AlSiO}_7)$) sodium aluminum silicate (NaAlSiO_4), calcium silicate (CaSiO_3) and perovskite CaTiO_3 as it is shown in Appendix A, Figure A2.

The experimental results from MW reductive roasting showed that although 5 min are enough for the full transformation of hematite to a mixture of magnetite and metallic iron the full transformation to metallic iron necessitates more time.

The 2nd cinder was again treated at optimum condition (0.6 kW and 1 L/min N₂ flow constant) in the microwave furnace due to the high absorption properties of Fe₃O₄ to allow the complete formation of metallic iron in the system.

The sample was transformed into tablets and placed inside the microwave furnace. As the previous microwave roasting process, an immediate absorption was detected causing an instantaneous incrementation of the temperature (reaching about 1250 °C). Furthermore, through the window of the pyrometer, light arcing phenomena that took place in some areas of the sample were observed. Due to these phenomena the recorded temperature locally reached around 1400 °C (Figure 10). The presence of these hot spots in the tablet depends on the interaction of metal iron, already present in the sample, with the microwave which creates a micro-arcing process [5,9,10,55,56].

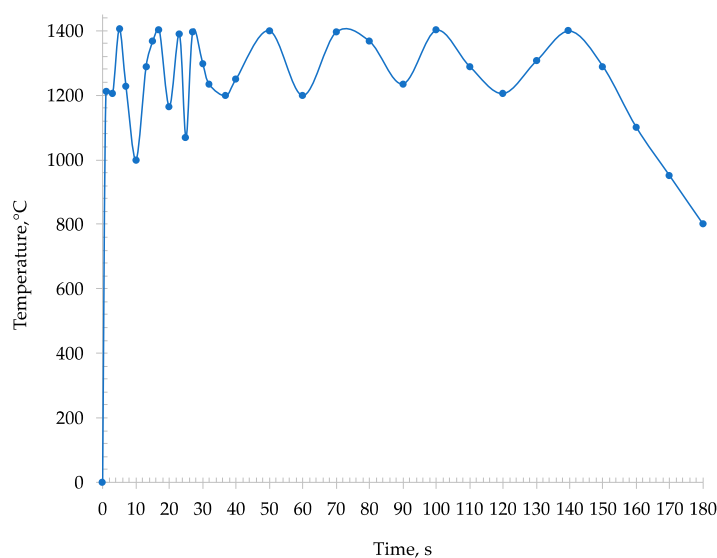


Figure 10. Heating rates of 3rd MW roasting process at 0.6 kW, 1 L/min N₂ flow constant and 180 s.

After 180 s, a drastically reduction of T was detected from the pyrometer (Figure 10) [2,10] and the experiments were stopped as the tablet reflected the microwave energy due to the increased concentration of conductive material (such as metallic iron).

From the comparison of the XRD profile of the cinder after the 1st microwave roasting reduction (1st MW), the cinder after the 2nd microwave roasting reduction (2nd MW) and the cinder after the 3rd microwave roasting reduction (3rd MW), it is possible to observe that metallic iron (Fe⁰) is the main iron mineralogical phases in the last MW stage. In the 2-theta range of 22 to 28°, the mineralogical characterization revealed that the hump related to the formation of a glassy region consisting of calcium silicate (CaSiO₃) and anorthite (CaAl₂SiO₃), is more evident, due to the high temperature reached during the 3rd MW roasting reduction. The other elements are present in the mixed forms of gehlenite (Ca₂Al(AlSiO₇)), sodium aluminum silicate (NaAlSiO₄), and perovskite CaTiO₃ as it is shown in Figure 11 [57].

To confirm the incrementation of the metallic iron content in each sample of the whole microwave roasting reduction (1st, 2nd and 3rd MW process), the above mentioned Zhiyong Xu method was used [54].

As it can be seen from the results shown in Table 7, after each microwave roasting reduction the percentage of the metallic iron present in the sample increased, comparing with the total amount of Fe.

The 3rd MW cinder was collected due to its strong magnetic properties and was treated through a CarpcoTM wet high intensity magnetic separator (WHIMS).

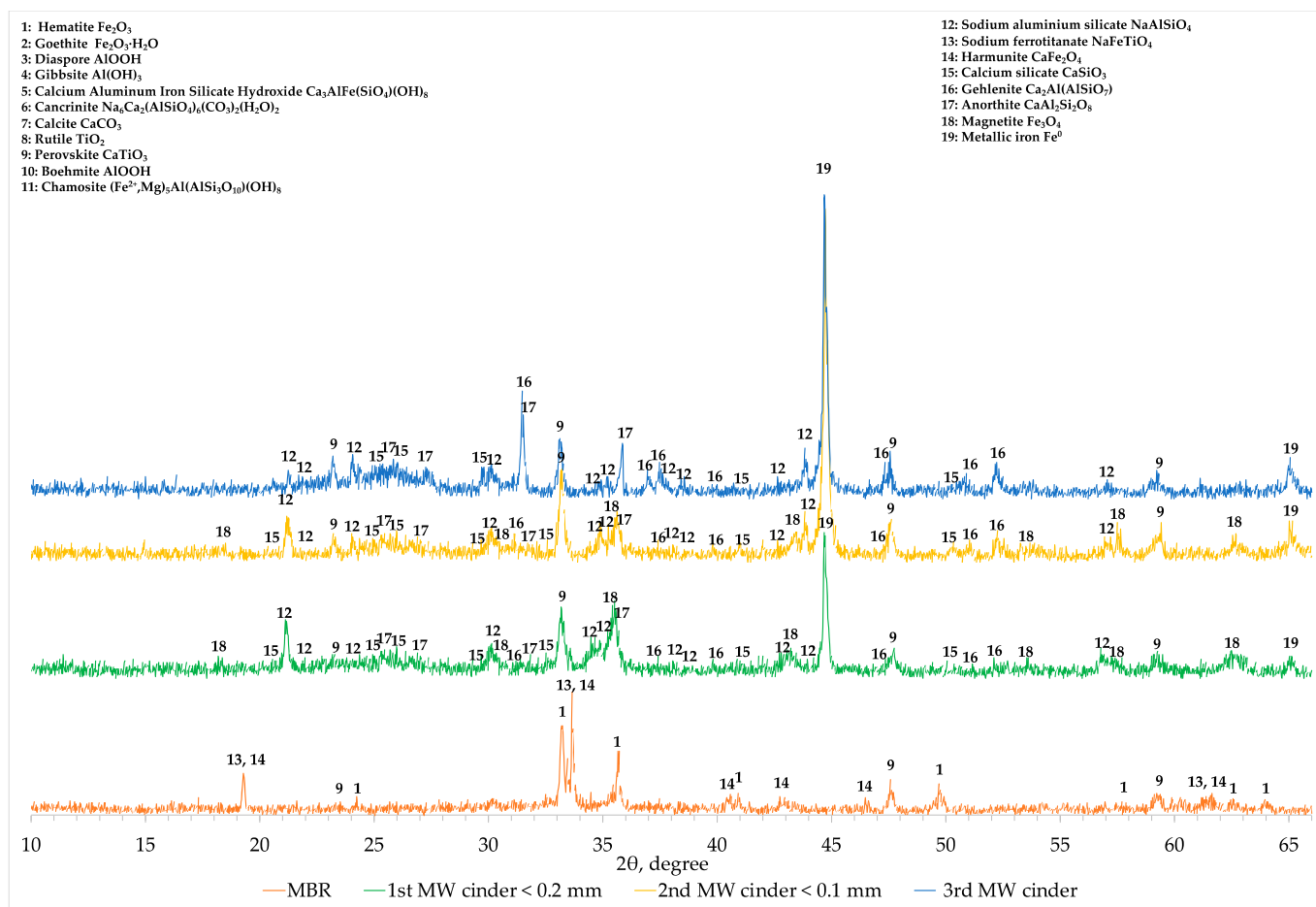


Figure 11. Comparison of the XRD spectra of modified BR (MBR), cinder after 1st microwave roasting reduction, cinder after 2nd microwave roasting reduction and cinder after 3rd microwave roasting reduction.

Table 7. Percentage of metallic iron/total iron content of modified BR and the three microwave cinders determined with Zhiyong Xu method.

Sample	% Fe ⁰ /Fe _{tot}
MBR	0.2
1st MW cinder	69
2nd MW cinder	85
3rd MW cinder	98

3.4. Magnetic Separation Process

The purposes of the magnetic separation are to liberate from the cinder the iron based components from the matrix and to concentrate them in the magnetic product.

To achieve these aims, the cinder was dispersed in water and was treated through the WHIMS two times following the procedure described in paragraph Material and Method.

Three different products (MAG I, MAG II, and NM) were collected, and representative samples were analyzed. MAG I represented the 62 wt.% of the 3rd MW cinder whereas MAG II was the 17 wt.% and NM the 21 wt.%

The three fractions were treated with Zhiyong Xu method to investigate the percentage of metallic iron in the sample comparing with the total amount of Fe. The results showed that in all the magnetic fractions, the iron analyzed was almost completely in form of metallic iron (about 98%).

As it can be seen from chemical analysis shown in Table 8, the MAG I is mainly concentrated in iron, while calcium, silicon, titanium are present in minor amount. Aluminum

is around 2 wt.% and Na content is negligible. On the other hand, in the NM fraction metallic iron is still present (4 wt.%), whereas the concentration of the other elements that composed the matrix is substantially higher.

Table 8. Chemical analysis of the cinder (3rd MW) and the three fractions (MAG I, MAG II, and NM) after the magnetic separation.

Sample	Fe	Al	Si	Ti	Na	Ca
3rd MW cinder	37.90	4.76	4.00	4.49	3.55	10.49
MAG I wt.%	55.29	1.51	1.59	2.40	0.49	6.67
MAG II wt.%	18.42	6.90	6.13	7.21	7.66	16.02
NM wt.%	2.94	12.47	9.29	8.38	9.19	17.22

The XRD comparison of 3rd MW cinder, MAG I, MAG II, and NM is presented in Figure 12. In MAG I the main peak is related to metallic iron, while the other mineralogical phases (gehlenite, calcium titanate, and anorthite) are detected with low intensity. Moreover, between 22 to 28° the characteristic hump associated to calcium silicate and anorthite is not visible and the peaks attributed to sodium aluminum silicate disappear.

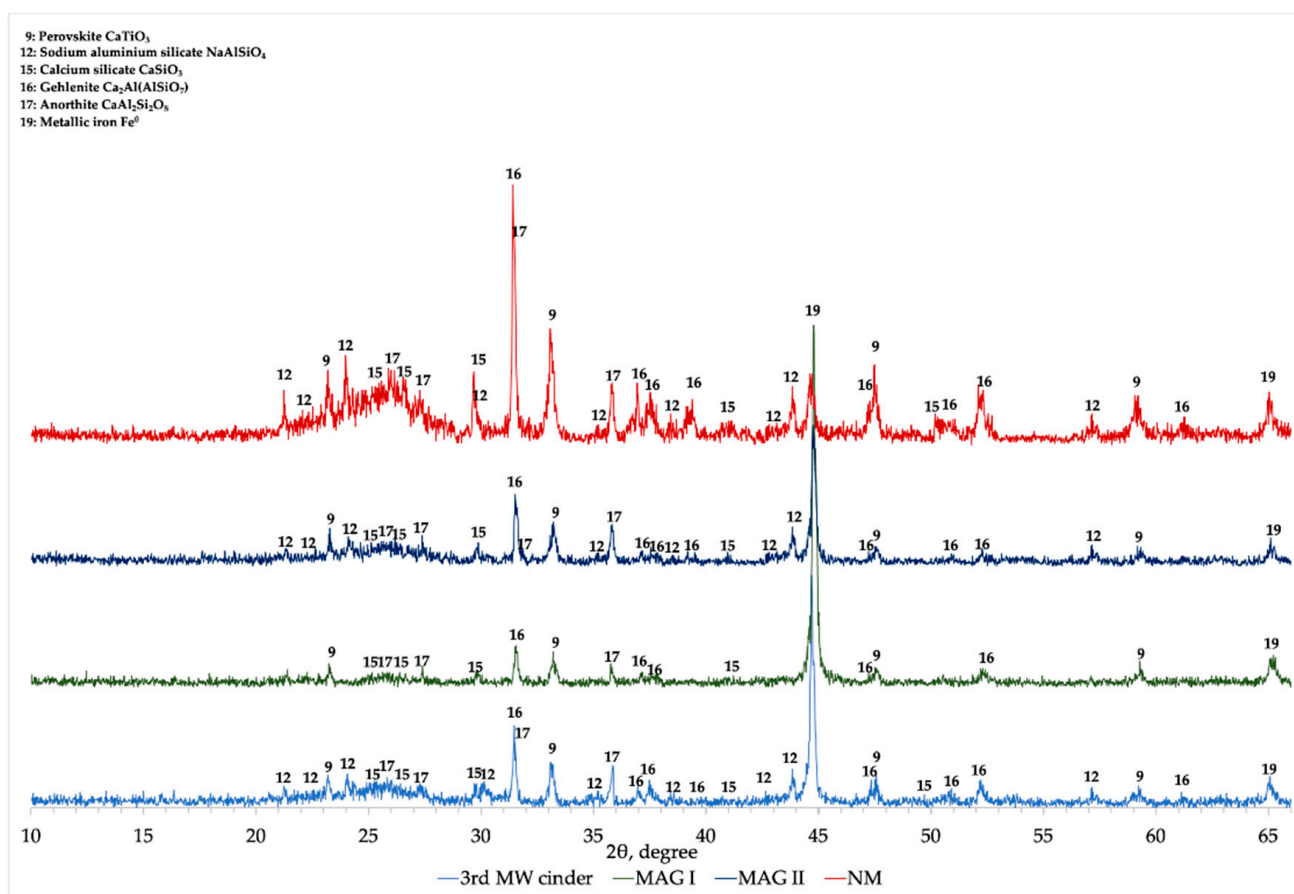


Figure 12. Comparison of the XRD profile of cinder after 3rd MW roasting process, magnetic fraction (MAG I), weak magnetic fraction (MAG II) and non-magnetic fraction (NM).

XRD analysis of NM fraction showed a different profile comparing with the one of MAG I. As it can be seen, the peak related to metallic iron (about 45°) is drastically reduced in intensity, while the hump associated to calcium silicate and anorthite is noticeable. Gehlenite and sodium aluminum silicate are detected with high intensity peaks.

Regarding MAG II, it is possible to notice that its mineralogical characterization is comparable to the initial cinder (LR 3rd MW).

SEM-EDS analysis of the three fractions confirmed the results of chemical and XRD analyses.

The back electron scattering macrograph of MAG I fraction (Figure 13) showed that the sample is composed by a melted metallic iron (Figure 13a) which has entrapped due to imperfect separation a solid matrix containing all the cinder constituents (Figure 13c). In addition, small particles with calcium titanate were detected also entrapped inside the metallic iron phase (Figure 13b).

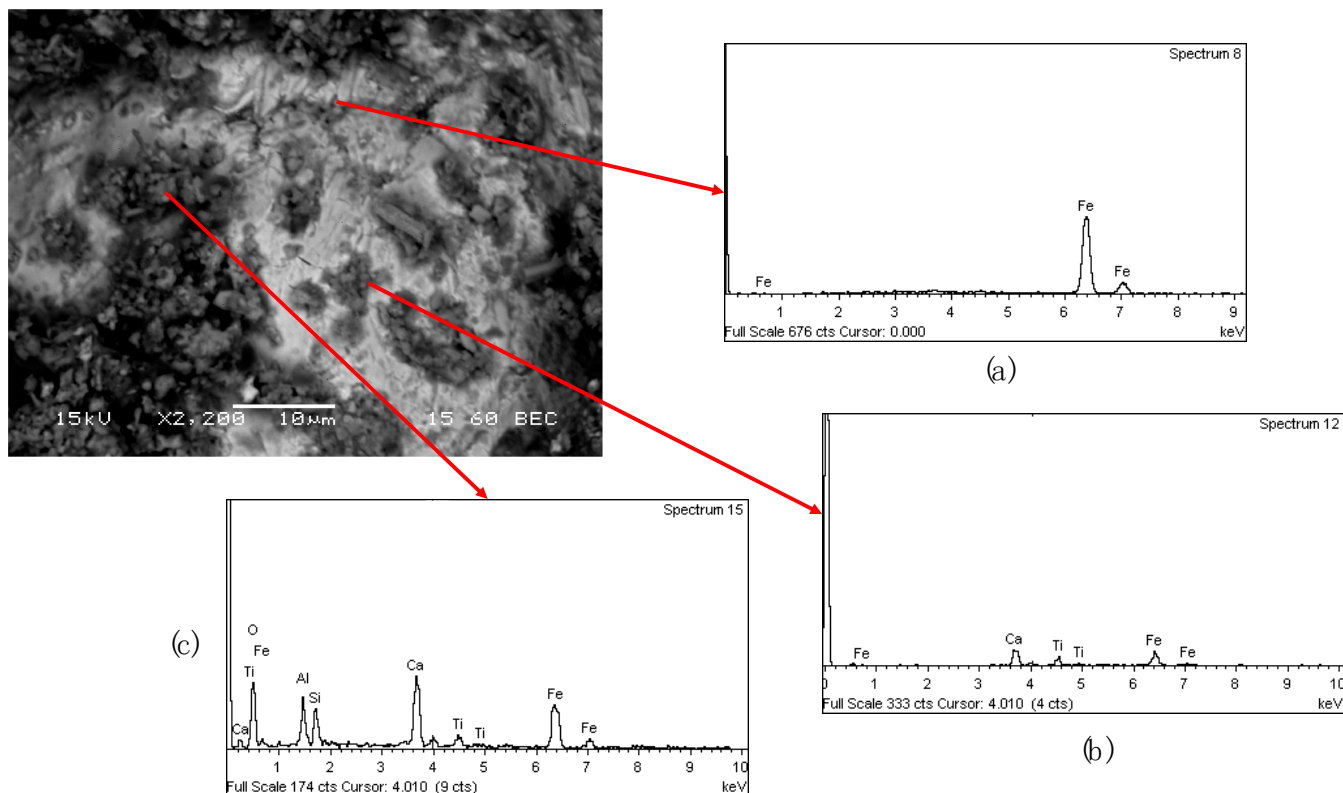


Figure 13. Back electron scattering mode SEM-EDS analysis of MAG I fraction: (a) melted metallic iron (b) calcium aluminium silicon oxide particles (c) particles composed of Si, Ca and Ti oxide mixture.

To understand the stratification of the different constituents of the sample, the area of sample shown in Figure 13 was studied through second electron imaging (SEI) mode. As it is observed in Figure 14, the particles containing the elements of the matrix are embedded on the melted metallic iron (dark substrate, Figure 14a) forming aggregates. Some particles were identified as calcium aluminum silicon oxide (Figure 14b), while some others were composed of Si, Ca, and Ti oxide mixture (Figure 14c).

The presence of Fe in the spectrum 1 (Figure 14c), is attributed to interferences from the metallic substrate, due the high magnification.

In Figure 15 the SEM analysis of the NM fraction with back electron scattering mode is shown. The image shows the presence of small metallic iron (Figure 15a) particles surrounded by light gray particles (calcium aluminum silicon oxide) (Figure 15b) and entrapped into dark gray area which was mainly composed by all the cinder constituents (Na, Al, Ca, Si, Ti, and Fe) (Figure 15c). Also, in this case, the presence of Fe in the spectra 3 and 4 (Figure 15b,c) is due to the interference from the metallic particles close to the detected area.

Furthermore, the NM fraction was analyzed by employing a secondary electron imaging mode to comprehend the existing different mineralogical phases (Figure 16).

Big particles composed with sodium aluminum silicate were identified (Figure 16d), in this grain also a calcium titanium phase (Figure 16c) and iron (Figure 16b) were detected. The presence of the other elements in the EDS-spectra depends on the proximity interference of the other mineralogical phases. Calcium aluminum silicate were found in a specific area of the sample (Figure 16a).

In conclusion, in terms of Fe partition within the different phases formed during the complex treatment of BR (Figure 17), after the 1st and 2nd microwave roasting reduction, nuggets were produced with high purity in Fe, overall extracting about 16% in the metallic iron spheres fraction with a particle size >0.2 mm and 2% in the spheres with a particle size >0.1 mm of the total Fe content of BR. Moreover, Fe was recovered through a magnetic separation process. Three fractions (MAG I, MAG II, and NM) were produced and analyzed. The Fe recovery within the MAG I was 69%, while it was 6% in MAG II and 1% in NM. The losses between bauxite residue and the sinter, and between the sinter and the modified bauxite residue are attributed to within experimental error margin of 5–10%.

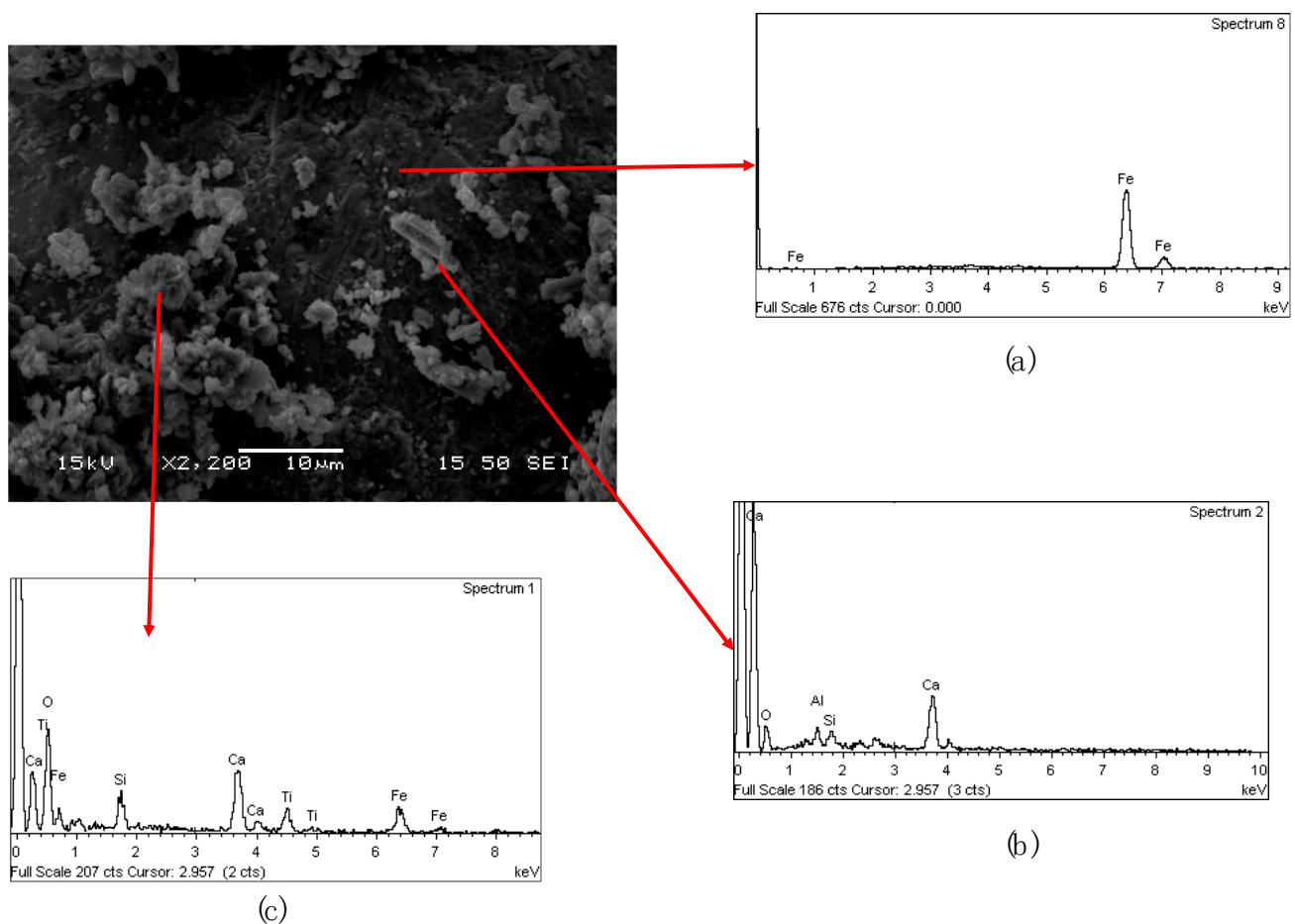


Figure 14. Secondary electron imaging mode SEM-EDS analysis of MAG I fraction: (a) melted metallic iron (b) calcium aluminium silicon oxide particles (c) particles composed of Si, Ca and Ti oxide mixture.

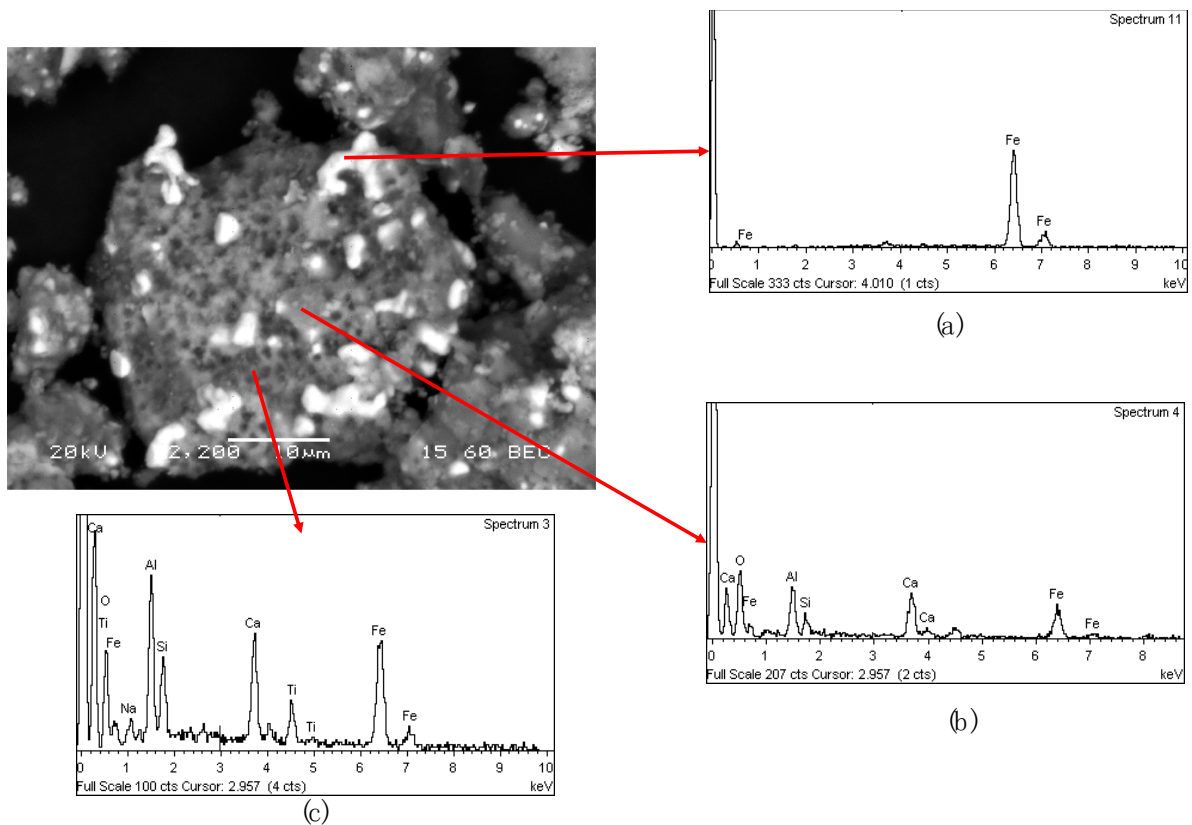


Figure 15. Back electron scattering mode SEM-EDS analysis of NM fraction: (a) small metallic iron particles (b) light gray particles (calcium aluminium silicon oxide) (c) particles composed by all the cinder constituents (Na, Al, Ca, Si, Ti and Fe).

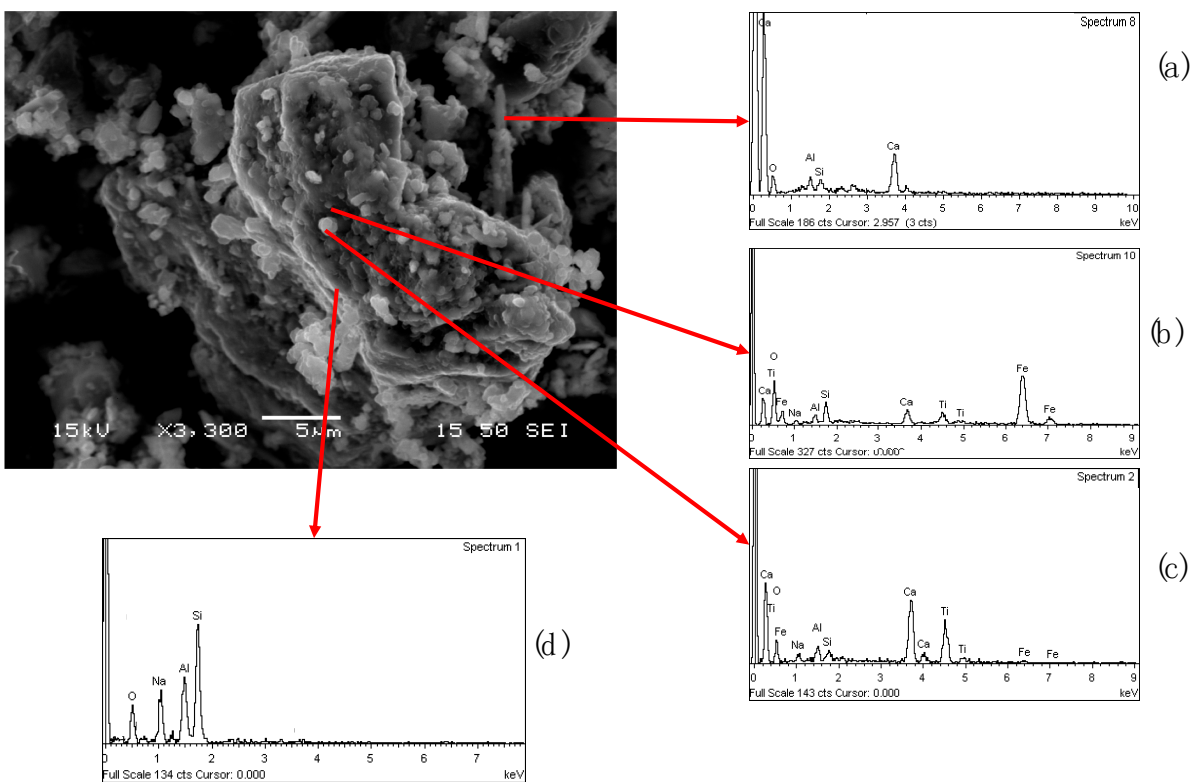


Figure 16. Secondary electron imaging mode SEM-EDS analysis of NM fraction: (a) calcium aluminium silicate particles (b) grains composed by iron (c) grains composed mainly by calcium titanium phase (d) sodium aluminium silicate.

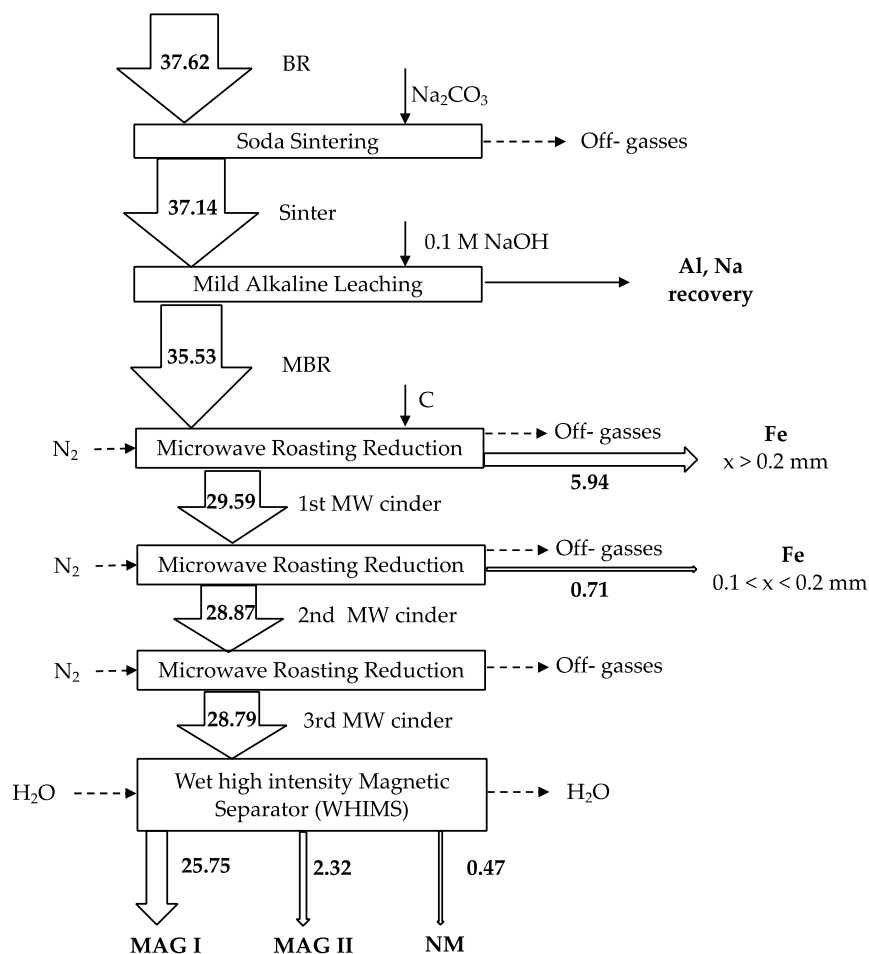


Figure 17. Mass distribution of Fe (g) based on chemical analysis data.

4. Conclusions

In this study, a combined soda sintering, and microwave reductive roasting process was presented to transform Fe³⁺ oxides contained in bauxite residue (hematite and goethite) into Fe²⁺ oxides (magnetite and wüstite) and metallic iron it was presented, avoiding the formation of hercynite. Figure 18 indicates the flowsheet of the combinations of aluminum and sodium recovery and carbothermic microwave roasting processes.

In the first step, all the alumina of BR were transformed into soluble sodium aluminates by adding 50% excess of sodium carbonate as flux followed by alkaline leaching to recover alumina.

Subsequently, the leached residue was mixed with carbon and treated in the microwave furnace at optimum conditions (0.6 kW and 0.225 C/MBR with 1 L/min N₂ flow constant for 300 s) for three times.

During the 1st and 2nd MW reductive roasting process the cinders resulted to be rich of spherical metallic Fe particles entrapped in the matrix which were separated by employing a manual sieve.

As a result of presence of the 3rd MW roasting reduction was the production of a cinder with magnetic properties. The cinder was subjected to a wet high intensity magnetic process and three different products (MAG I, MAG II, and NM) were collected.

As a result of magnetic separation, higher concentration of metallic iron was detected in MAG I (56 wt.%), even though calcium, silicon and titanium were still present in minor amount. SEM and XRD analysis of the non-magnetic fraction (NM) revealed the existence of metallic iron particles (about 4 wt.%) embedded on the ceramic matrix.

It can be concluded that the combined process presented is a favorable approach to recover iron comparing with a previous works [19,20,31]. In addition, an added value of

this process is also the recovery of aluminum (70% of aluminum recovered) after the alkali leaching in the first step.

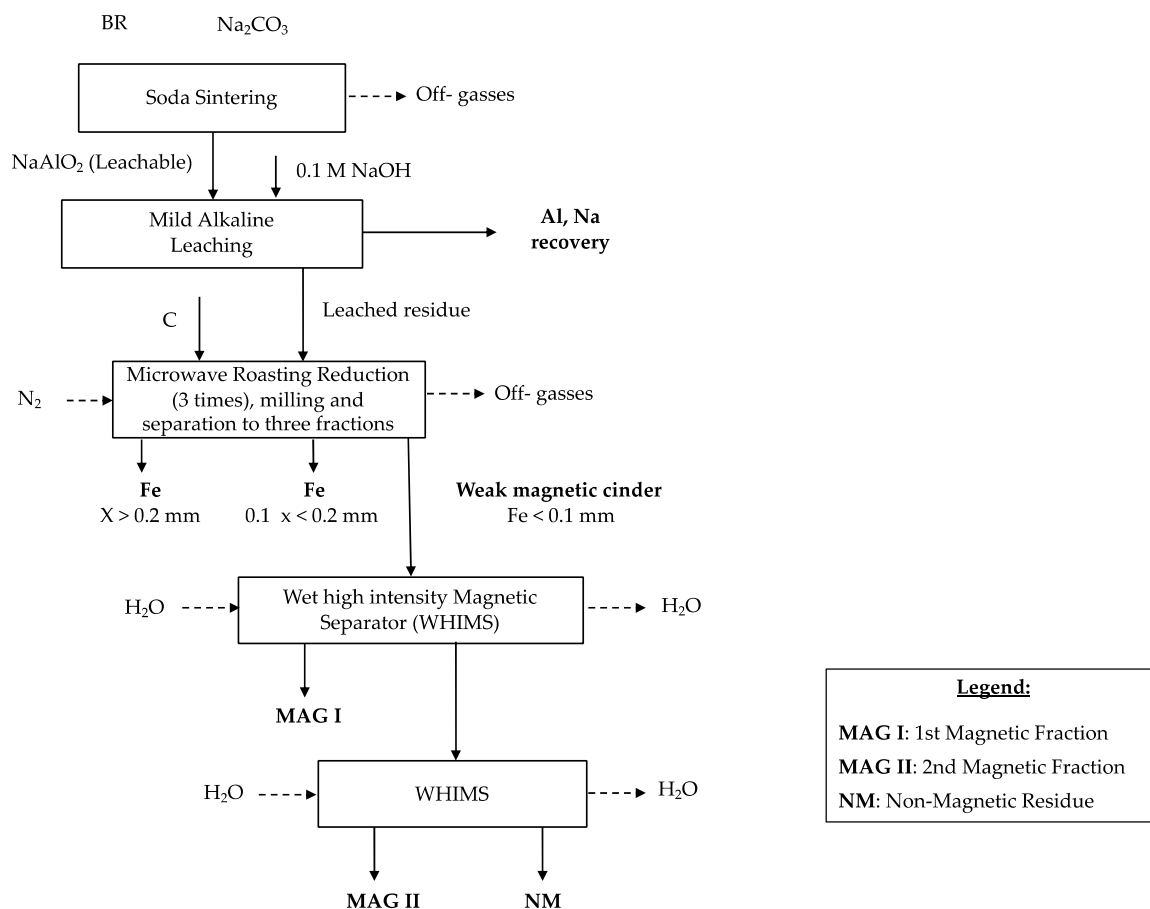


Figure 18. Flowsheet of the combinations of soda sintering and carbothermic microwave roasting processes.

In terms of Fe recovery, after the 1st and 2nd MW roasting reduction, nuggets were produced with high purity in Fe, overall extracting about 16% in the fraction with a particle size > 0.2 mm and 2% in the fraction with particle size > 0.1 mm of the total Fe content of BR. Moreover, an advantage of this procedure is that Fe nuggets are easily recoverable through physical separation. Thereafter the 3rd MW roasting reduction, Fe was recovered through the magnetic separation process and attested to 69% in MAG I, while it was 6% in MAG II and 1% in NM.

MAG I contains almost 55% metallic iron and have as impurities calcium aluminosilicates as well as perovskite. It is an upgraded material in comparison with BR and can be added in the electric arc furnaces of secondary steel production as a raw material together with scrap. The impurities can play the role of fluxes for formation of the $\text{CaO-SiO}_2\text{-Al}_2\text{O}_3$ type slag. In addition to MAG I, the Fe nuggets separated from the first two MW treatments can be also added in EAF for iron recovery. The nuggets have a purity in metallic iron higher than 93% and the impurities are also aluminosilicates. Therefore, with the combined soda roasting and MW carbothermic roasting process almost 87% of iron contained in BR is recovered as impure metallic iron and 70% of contained aluminum is recovered in the form of a sodium aluminate solution which can be recycled in the Bayer process for alumina production.

As a final conclusion the combined soda roasting and MW carbothermic roasting process could be potentially developed into a high throughput continuous process to valorize BR and make it a secondary raw material resource.

Author Contributions: Conceptualization and design the experiments, C.C., E.B., P.W.Y.T., and D.P.; C.C. performed the microwave and magnetic separation experiments; Writing—original draft preparation and investigation, P.W.Y.T. performed the soda sintering process; Writing—review and editing and investigation; C.C. and P.W.Y.T. performed XRD and SEM-EDS and analyzed the data; Data validation, software training and further conceptualization of project, E.B. and D.P.; Writing—review and editing, E.B. and D.P.; Supervision, E.B. and D.P.; Project administration and funding acquisition, D.P. All authors have read and agreed to the published version of the manuscript.

Funding: (1) Research leading to these results has received funding from the European Community’s Horizon 2020 Program ([H2020/2014–2019]) under Grant Agreements no. 636876 (MSCA-ETN REDMUD) and no. 776469 (Removal). This publication reflects only the authors’ view, exempting the Community from any liability. Project website: <http://www.etn.redmud.org> (accessed on 4 January 2021). (2) Research leading to these results has received funding from the European Community’s Horizon 2020 Programme (H2020/2014–2019) under Grant Agreement No. 776469 (REMOVAL). This publication reflects only the author’s view, exempting the Community from any liability. Project website: <https://www.removal-project.com/> (accessed on 4 January 2021).

Data Availability Statement: Not applicable.

Acknowledgments: Special thanks to National Technical University of Athens (NTUA) team for the immeasurable support.

Conflicts of Interest: The authors declare no conflict of interest.

Appendix A

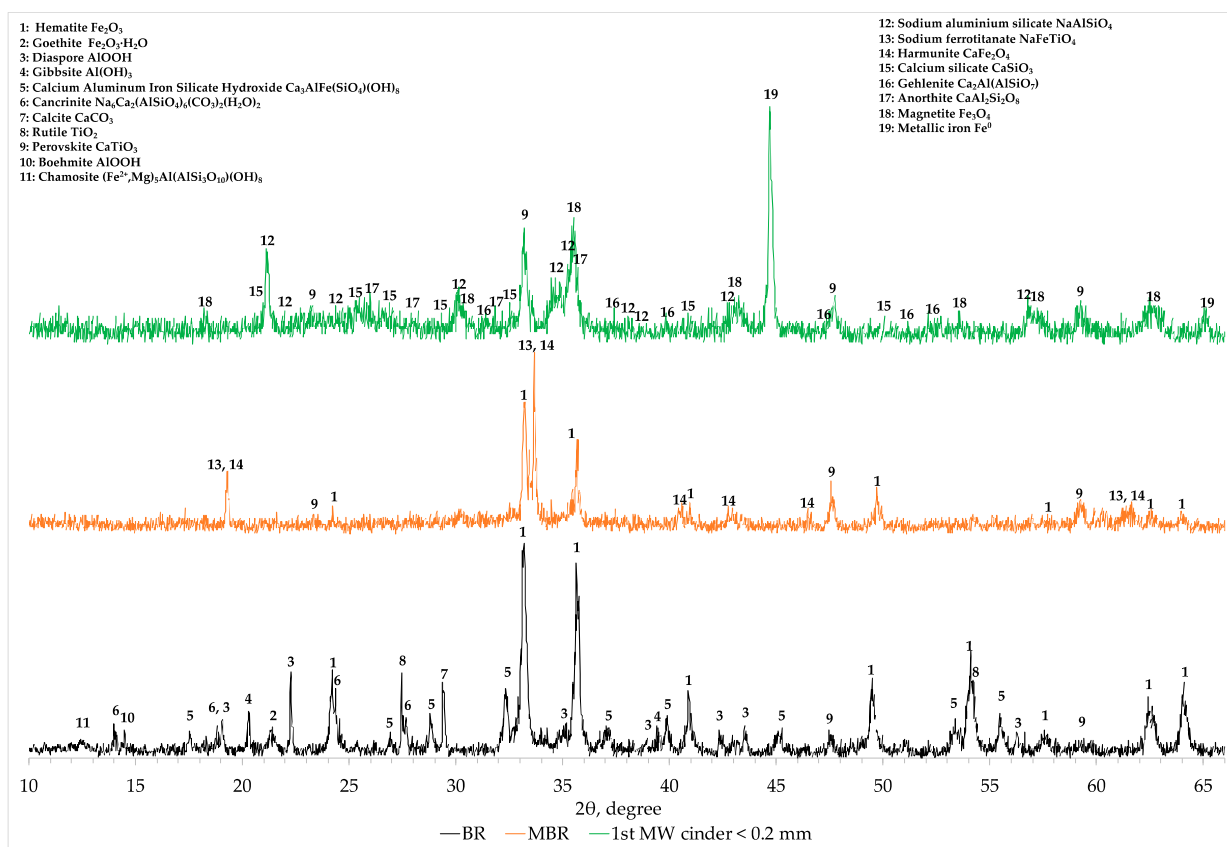


Figure A1. Comparison of XRD profiles of bauxite residue, modified BR and 1st cinder fraction with particle size <0.2 mm.

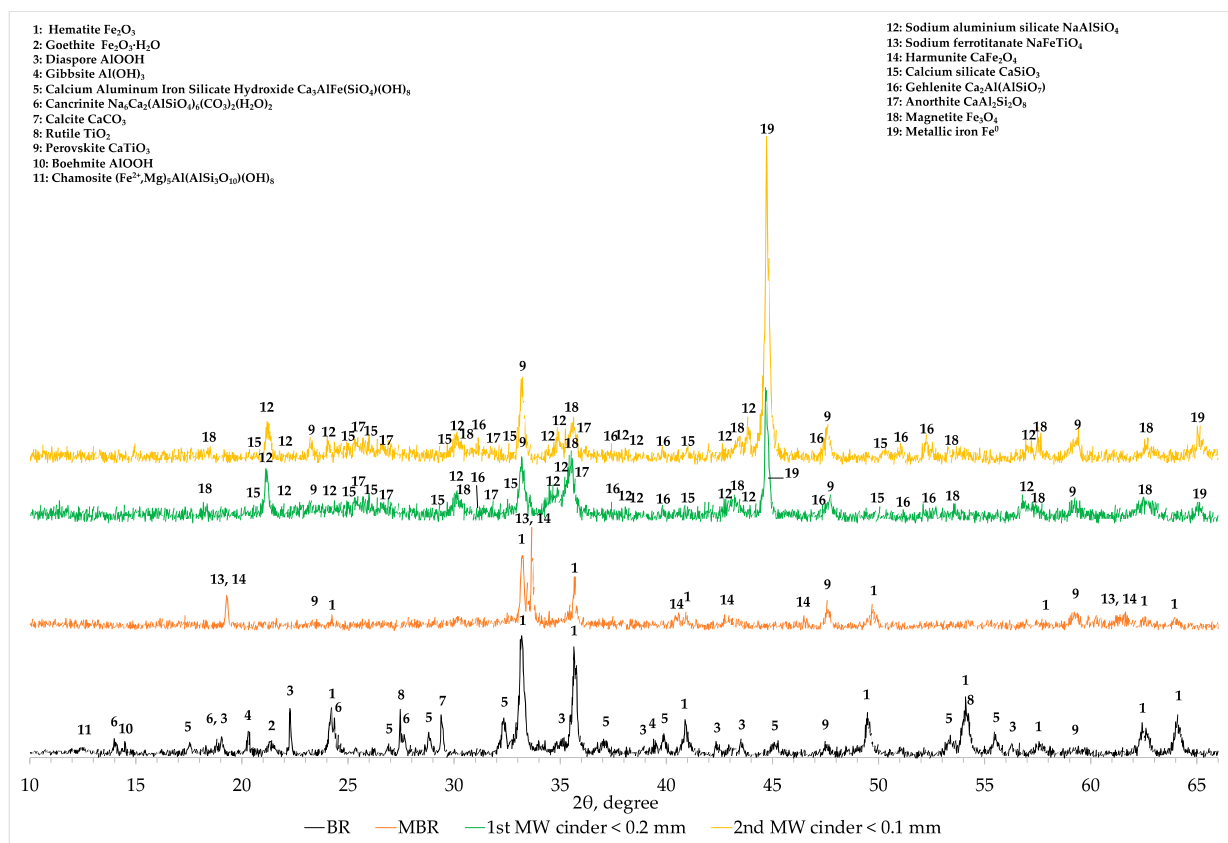


Figure A2. XRD Comparison between BR, MBR, cinder after 1st microwave roasting reduction and cinder after 2nd microwave roasting reduction.

References

- Javad, S.; Barani, K. Microwave Heating Applications in Mineral Processing. In *The Development and Application of Microwave Heating*; IntechOpen: Rijeka, Croatia, 2012; pp. 79–104.
- Meredith, R. Engineers' Handbook of Industrial Microwave Heating. In *Engineers' Handbook of Industrial Microwave Heating*; Institution of Engineering and Technology (IET): London, UK, 1998; p. 382.
- Lovas, M.; Znamenackova, I.; Zubrik, M.; Kovacova, M.; Dolinska, S. The application of microwave energy in mineral processing—A review. *Rocnik* **2011**, *16*, 137–148.
- Jones, D.; Lelyveld, T.; Mavrofidis, S.; Kingman, S.; Miles, N. Microwave heating applications in environmental engineering—A review. *Resour. Conserv. Recycl.* **2002**, *34*, 75–90. [[CrossRef](#)]
- Pickles, C. Microwaves in extractive metallurgy: Part 2—A review of applications. *Miner. Eng.* **2009**, *22*, 1112–1118. [[CrossRef](#)]
- Metaxas, A.C.; Meredith, R.J. *Industrial Microwave Heating*; Institution of Engineering and Technology (IET): London, UK, 1988; Volume 29.
- Menéndez, J.; Arenillas, A.; Fidalgo, B.; Fernández, Y.; Zubizarreta, L.; Calvo, E.; Bermúdez, J. Microwave heating processes involving carbon materials. *Fuel Process. Technol.* **2010**, *91*, 1–8. [[CrossRef](#)]
- Dorn, C.; Behrend, R.; Giannopoulos, D.; Napolano, L.; Baños, B.G.; James, V.; Uhlig, V.; Catalá, J.; A Founti, M.; Trimis, D. KPI and LCA Evaluation of Integrated Microwave Technology for High Temperature Processes. *Procedia CIRP* **2015**, *29*, 492–497. [[CrossRef](#)]
- Standish, N.; Worner, H. Microwave Application in the Reduction of Metal Oxides with Carbon. *J. Microw. Power Electromagn. Energy* **1990**, *25*, 177–180. [[CrossRef](#)]
- Haque, K.E. Microwave energy for mineral treatment processes—A brief review. *Int. J. Miner. Process.* **1999**, *57*, 1–24. [[CrossRef](#)]
- Hertel, T.; Cardenia, C.; Balomenos, E.; Pnias, D.; Pontikes, Y. Microwave treatment of bauxite residue for the production of inorganic polymers. In Proceedings of the 2nd International Bauxite Residue Valorisation and Best Practices Conference, Athens, Greece, 7–10 May 2018.
- Agrawal, S.; Rayapudi, V.; Dhawan, N. Microwave Reduction of Red Mud for Recovery of Iron Values. *J. Sustain. Met.* **2018**, *4*, 427–436. [[CrossRef](#)]
- Agrawal, S.; Rayapudi, V.; Dhawan, N. Comparison of microwave and conventional carbothermal reduction of red mud for recovery of iron values. *Miner. Eng.* **2019**, *132*, 202–210. [[CrossRef](#)]

14. Agrawal, S.; Dhawan, N. Investigation of carbothermic microwave reduction followed by acid leaching for recovery of iron and aluminum values from Indian red mud. *Miner. Eng.* **2020**, *159*, 106653. [[CrossRef](#)]
15. Samouhos, M.; Taxiarchou, M.; Tsakiridis, P.E.; Potiriadis, K. Greek “red mud” residue: A study of microwave reductive roasting followed by magnetic separation for a metallic iron recovery process. *J. Hazard. Mater.* **2013**, 193–205. [[CrossRef](#)] [[PubMed](#)]
16. Zhang, J.; Guo, Q.; Tian, C.; Zhan, W.; Chen, S.; He, Z. High-efficiency preparation of Fe–Al based flocculants from red mud by microwave selective carbothermic reduction and magnetic separation. *Environ. Prog. Sustain. Energy* **2020**, *39*. [[CrossRef](#)]
17. Evans, K. The History, Challenges, and New Developments in the Management and Use of Bauxite Residue. *J. Sustain. Met.* **2016**, *2*, 316–331. [[CrossRef](#)]
18. Rai, S.; Bahadure, S.; Chaddha, M.J.; Agnihotri, A. Disposal Practices and Utilization of Red Mud (Bauxite Residue): A Review in Indian Context and Abroad. *J. Sustain. Met.* **2020**, *6*, 1–8. [[CrossRef](#)]
19. Cardenia, C.; Balomenos, E.; Panias, D. Iron Recovery from Bauxite Residue Through Reductive Roasting and Wet Magnetic Separation. *J. Sustain. Met.* **2018**, *5*, 9–19. [[CrossRef](#)]
20. Cardenia, C.; Xakalash, B.; Balomenos, E.; Panias, D.; Friedrich, B. Reductive Roasting Process for the Recovery of Iron Oxides from Bauxite Residue through Rotary Kiln Furnace and Magnetic Separation. In Proceedings of the 35th Int ICSOBA Conference, Hamburg, Germany, 2–5 October 2017; pp. 595–602.
21. Xenidis, A.; Zografidis, C.; Kotsis, I.; Boufounos, D. Reductive roasting and magnetic separation of Greek bauxite residue for its utilization in iron ore industry. *TMS Light Met.* **2009**, 63–67.
22. Zhu, D.-Q.; Chun, T.-J.; Pan, J.; Zhen, H.E. Recovery of Iron From High-Iron Red Mud by Reduction Roasting With Adding Sodium Salt. *J. Iron Steel Res. Int.* **2012**, *19*, 1–5. [[CrossRef](#)]
23. Agrawal, S.; Rayapudi, V.; Dhawan, N. Extraction of Iron values from Red mud. *Mater. Today: Proc.* **2018**, *5*, 17064–17072. [[CrossRef](#)]
24. Liu, Y.; Naidu, R. Hidden values in bauxite residue (red mud): Recovery of metals. *Waste Manag.* **2014**, *34*, 2662–2673. [[CrossRef](#)] [[PubMed](#)]
25. Kumar, S.; Kumar, R.; Bandopadhyay, A. Innovative methodologies for the utilisation of wastes from metallurgical and allied industries. *Resour. Conserv. Recycl.* **2006**, *48*, 301–314. [[CrossRef](#)]
26. Valeev, D.; Zinoveev, D.; Kondratiev, A.; Lubyanoi, D.; Pankratov, D. Reductive Smelting of Neutralized Red Mud for Iron Recovery and Produced Pig Iron for Heat-Resistant Castings. *Metals* **2019**, *10*, 32. [[CrossRef](#)]
27. Jayasankar, K.; Ray, P.K.; Chaubey, A.K.; Padhi, A.; Satapathy, B.K.; Mukherjee, P.S. Production of pig iron from red mud waste fines using thermal plasma technology. *Int. J. Miner. Met. Mater.* **2012**, *19*, 679–684. [[CrossRef](#)]
28. Borra, C.R.; Blanpain, B.; Pontikes, Y.; Binnemans, K.; Van Gerven, T. Smelting of Bauxite Residue (Red Mud) in View of Iron and Selective Rare Earths Recovery. *J. Sustain. Met.* **2015**, *2*, 28–37. [[CrossRef](#)]
29. Balomenos, E.; Gianopoulou, I.; Panias, D.; Paspaliaris, I.; Perry, K.; Boufounos, D. Efficient and Complete Exploitation of the Bauxite Residue (Red Mud) Produced in the Bayer Process. *Proc. EMC 2011* **2011**, 745–758.
30. Ning, G.; Zhang, B.; Liu, C.; Li, S.; Ye, Y.; Jiang, M. Large-Scale Consumption and Zero-Waste Recycling Method of Red Mud in Steel Making Process. *Minerals* **2018**, *8*, 102. [[CrossRef](#)]
31. Cardenia, C.; Balomenos, E.; Panias, D. Optimization of Microwave Reductive Roasting Process of Bauxite Residue. *Metals* **2020**, *10*, 1083. [[CrossRef](#)]
32. Lu, T.; Pickles, C.A.; Kelebek, S. Carbothermal Reductive Upgrading of a Bauxite Ore Using Microwave Radiation. *High Temp. Mater. Process.* **2012**, *31*, 139–148. [[CrossRef](#)]
33. Fukushima, J.; Hayashi, Y.; Takizawa, H. Structure and magnetic properties of FeAl₂O₄ synthesized by microwave magnetic field irradiation. *J. Asian Ceram. Soc.* **2013**, *1*, 41–45. [[CrossRef](#)]
34. Kaußen, F.M.; Friedrich, B. Methods for Alkaline Recovery of Aluminum from Bauxite Residue. *J. Sustain. Met.* **2016**, *2*, 353–364. [[CrossRef](#)]
35. Kaußen, F.M.; Sofras, I.; Friedrich, B. Carbothermic reduction of red mud in an EAF and subsequent recovery of aluminum from the slag by pressure leaching in caustic solution. In Proceedings of the Bauxite Residue Valorisation and Best Practices (BR 2015), Leuven, Belgium, 29 September 2020; pp. 185–189.
36. Zheng, K.; Gerson, A.R.; Addai-Mensah, J.; Smart, R.S. The influence of sodium carbonate on sodium aluminosilicate crystallisation and solubility in sodium aluminate solutions. *J. Cryst. Growth* **1997**, *171*, 197–208. [[CrossRef](#)]
37. Alp, A.; Aydin, A. The Investigation of Efficient Conditions for Alumina Production from Diasporic Bauxites. *Can. Met. Q.* **2002**, *41*, 41–46. [[CrossRef](#)]
38. Meher, S.N.; Rout, A.K.; Padhi, B.K. Extraction of Alumina from Red Mud by Divalent Alkaline Earth Metal Soda Ash Sinter Process. In *Light Metals 2011*; John Wiley & Sons, Inc.: Hoboken, NJ, USA, 2011; pp. 231–236.
39. Meher, S.N.; Padhi, B. A novel method for extraction of alumina from red mud by divalent alkaline earth metal oxide and soda ash sinter process. *Int. J. Environ. Waste Manag.* **2014**, *13*, 231. [[CrossRef](#)]
40. Tam, P.W.Y.; Panias, D.; Vassiliadou, V. Tam Sintering Optimisation and Recovery of Aluminum and Sodium from Greek Bauxite Residue. *Minerals* **2019**, *9*, 571. [[CrossRef](#)]
41. Gräfe, M.; Power, G.; Klauber, C. Bauxite residue issues: III. Alkalinity and associated chemistry. *Hydrometallurgy* **2011**, *108*, 60–79. [[CrossRef](#)]
42. Kaußen, F.; Friedrich, B. Reductive Smelting of Red Mud for Iron Recovery. *Chem. Ing. Tech.* **2015**, *87*, 1535–1542. [[CrossRef](#)]

43. Kaußen, F.; Friedrich, B. Phase characterization and thermochemical simulation of (landfilled) bauxite residue (“red mud”) in different alkaline processes optimized for aluminum recovery. *Hydrometallurgy* **2018**, *176*, 49–61. [[CrossRef](#)]
44. Anisonyan, K.G.; Kopyev, D.Y.; Goncharov, K.V.; Sadykhov, G.B. An investigation of a single-stage red mud reducing roasting process with the cast iron and aluminate slag production. *Non-Ferrous Met.* **2018**, 18–23. [[CrossRef](#)]
45. Tam, P.; Yin, W.; Kakalash, B.; Friedrich, B.; Panias, D. Carbothermic Reduction of Bauxite Residue for Iron Recovery and Subsequent Aluminium Recovery from Slag Leaching. In Proceedings of the 35th Int ICSOBA Conference, Hamburg, Germany, 2–5 October 2017; pp. 603–614.
46. Tam, P.W.Y.; Cardenia, C.; Kakalash, B.; Vassiliadou, V.; Panias, D.; Friedrich, B. Conceptual flowsheets for combined recovery of Fe and Al from bauxite residue. In Proceedings of the 2nd International Bauxite Residue Valorisation and Best Practices Conference, Athens, Greece, 7–10 May 2018.
47. Li, X.-B.; Xiaobin, L.; Liu, W.; Liu, G.-H.; Peng, Z.-H.; Zhou, Q.-S.; Qi, T.-G. Recovery of alumina and ferric oxide from Bayer red mud rich in iron by reduction sintering. *Trans. Nonferrous Met. Soc. China* **2009**, *19*, 1342–1347. [[CrossRef](#)]
48. Liu, W.; Sun, S.; Zhang, L.; Jahanshahi, S.; Yang, J. Experimental and simulative study on phase transformation in Bayer red mud soda-lime roasting system and recovery of Al, Na and Fe. *Miner. Eng.* **2012**, *39*, 213–218. [[CrossRef](#)]
49. Zinoveev, D.; Grudinsky, P.; Zakunov, A.; Semenov, A.; Panova, M.; Valeev, D.; Kondratiev, A.; Dyubanov, V.; Petelin, A.; Valeev, D. Influence of Na₂CO₃ and K₂CO₃ Addition on Iron Grain Growth during Carbothermic Reduction of Red Mud. *Metals* **2019**, *9*, 1313. [[CrossRef](#)]
50. Li, G.; Liu, M.; Rao, M.; Jiang, T.; Zhuang, J.; Zhang, Y. Stepwise extraction of valuable components from red mud based on reductive roasting with sodium salts. *J. Hazard. Mater.* **2014**, *280*, 774–780. [[CrossRef](#)]
51. Grudinsky, P.; Zinoveev, D.; Pankratov, D.; Semenov, A.; Panova, M.; Kondratiev, A.; Zakunov, A.; Dyubanov, V.; Petelin, A. Influence of Sodium Sulfate Addition on Iron Grain Growth during Carbothermic Roasting of Red Mud Samples with Different Basicity. *Metals* **2020**, *10*, 1571. [[CrossRef](#)]
52. Suprpto, S.; Istiqomah, Z.; Santoso, E.; Dawam, A.A.; Prasetyoko, D. Alumina Extraction from Red Mud by Magnetic Separation. *Indones. J. Chem.* **2018**, *18*, 331. [[CrossRef](#)]
53. Wei, D.; Jun-Hui, X.; Yang, P.; Si-Yue, S.; Tao, C. Iron Extraction from Red Mud using Roasting with Sodium Salt. *Miner. Process. Extr. Met. Rev.* **2019**, 1–9. [[CrossRef](#)]
54. Xu, Z.; Hwang, J.; Greenlund, R.; Huang, X.; Luo, J.; Anschuetz, S. Quantitative Determination of Metallic Iron Content in Steel-Making Slag. *J. Miner. Mater. Charact. Eng.* **2003**, *2*, 65–70. [[CrossRef](#)]
55. Pickles, C. Microwaves in extractive metallurgy: Part 1—Review of fundamentals. *Miner. Eng.* **2009**, *22*, 1102–1111. [[CrossRef](#)]
56. Thostenson, E.; Chou, T.-W. Microwave processing: Fundamentals and applications. *Compos. Part A: Appl. Sci. Manuf.* **1999**, *30*, 1055–1071. [[CrossRef](#)]
57. Sglavo, V.M.; Campostrini, R.; Maurina, S.; Carturan, G.; Monagheddu, M.; Budroni, G.; Cocco, G. Bauxite ‘red mud’ in the ceramic industry. Part 1: Thermal behaviour. *J. Eur. Ceram. Soc.* **2000**, *20*, 235–244. [[CrossRef](#)]